Wireless Brain-Computer Interface for Wheelchair Control by Using Fast Machine Learning and Real-Time Hyper-Dimensional Classification

Valerio F. Annese[1], Giovanni Mezzina[2], Daniela De Venuto[2]

[1] School of Engineering, University of Glasgow,
Glasgow G12 8TA, U.K.
{v.annese.1@research.gla.ac.uk}
[2] Dept. of Electrical and Information Engineering, Politecnico di Bari
Via Orabona 4, 70125 Bari, Italy
{daniela.devenuto@poliba.it}

Abstract. This paper presents a noninvasive brain-controlled P300-based wheelchair driven by EEG signals to be used by tetraplegic and paralytic users. The P300 - an Evoked Related Potential (ERP) - is induced for purpose by visual stimuli. The developed Brain-Computer Interface is made up by: (i) acquisition unit; (ii) processing unit and (iii) navigation unit. The acquisition unit is a wireless 32-channel EEG headset collecting data from 6 electrodes (parietal-cortex area). The processing unit is a dedicated µPC performing stimuli delivery, data gathering, Machine Learning (ML), real-time hyper-dimensional classification leading to the user intention interpretation. The ML stage is based on a custom algorithm (t-RIDE) which trains the following classification stage on the user-tuned P300 reference features. The real-time classification performs a functional approach for time-domain features extraction, which reduce the amount of data to be analyzed. The Raspberry-based navigation unit actuates the received commands and support the wheelchair motion using peripheral sensors (USB camera for video processing, ultrasound sensors). Differently from related works, the proposed protocol for stimulation is aware of the environment. The experimental results, based on a dataset of 5 subjects, demonstrate that: (i) the implemented ML algorithm allows a complete P300 spatio-temporal characterization in 1.95s using only 22 target brain visual stimuli (88s/direction); (ii) the complete classification chain (from features extraction to validation) takes in the worst case only 19.65ms ± 10.1, allowing real-time control; (iii) the classification accuracy of the implemented BCI is 80.5±4.1% on single-trial.

Keywords: BCI, Machine Learning, Classification, EEG, ERP, P300.

1 Introduction

Brain-Computer Interface (BCI) systems allow the user to control external devices, i.e. independent of peripheral nerves and muscles, with only brain signals. The first BCI system was implemented by W. Grey et al. in 1964 [1]. In [1], Grey et al. presented the development of a mind-controlled cursor. This work represents a milestone: the demonstration of the possibility of controlling devices with a specific brain signal belonging to the cognitive area fueled an exponential growth in the field of BCI.

Nowadays, BCI systems cover a wide range of applications [2-10] such as locomotion (wheelchair [2], car [3, 4] robot or neuro-prosthesis [5]), rehabilitation (the "Bionic Eye" [6]), communication (the P300 speller [7]), environmental control (the "Brain Gate" [8]) and entertaining (neuro-games [9]). Generally, they can be categorized basing on the particular Brain Activity Pattern (BAP) to be detected, i.e. sensorimotor rhythms (SMR), amplitude modulation of slow cortical potentials (SCP), visual cortex potentials (VEPs) or Event-Related Potentials (ERPs) [10]. Among the ERPs, the most commonly used potential for BCI applications is the P300. The P300 is a large positive deflection detectable in the EEGs when a rare stimulus ("target") is discriminated from multiple different frequent stimuli ("non-target"). This kind of stimuli delivery protocol is commonly known as "oddball paradigm" [11, 12]. The P300, reaching its peak around 300ms after the target stimulus, reflects the stage of stimulus classification and, for this reason, can be also used for diagnostic purpose [13, 14]. Although individual differences in P300 latency and amplitude have also been reported in [13], P300 is detectable for every human being, with a high degree of repeatability. In the field of BCI for locomotion, strong interest was shown in the implementation of brain controlled wheelchairs [15], due to the inestimable impact that this technology can have on the quality of life of paralytic, tetraplegic and motor impaired subjects. Despite the extensive research [2-10, 15], the high computational times to perform both machine learning (ML) and classification make the system very challenging in a real-life scenario. In this context, this paper presents a P300-based BCI for the brain-control a wheelchair i.e. without need for any physical interaction. Differently from SMR and SCP based BCI, the developed BCI bases its operation on the P300, which does not require intensive user training (P300 component results from endogenous attention-based brain function). Furthermore, P300-based BCIs generally achieve a higher detection rate [15]. The complete architecture is made up by three sub-systems: (i) the acquisition unit; (ii) the processing unit and (iii) the navigation unit. The main improvement of the proposed BCI systems with respect to the state of the art are: (i) the use of a novel custom algorithm (t-RIDE) for fast ML and (ii) a fully spatio-temporal features-based approach for the real-time hyper-dimensional classification, addressing the need for computational speed. In particular, the adaption of t-RIDE [3, 4, 11-14], for ML stage allows a complete P300 spatio-temporal characterization using only 22 target brain visual stimuli (88s for each addressable command). Additionally, the functional approach for the classification based on spatio-temporal features extraction (FE), allows fast interpretation of the user's intention (worst case: 19.65ms ± 10.1ms) keeping high success rate 89.54 % ±4.03 (tested on 5 subjects). Section II outlines the architecture of the BCI system, focusing on each sub-system composing the architecture. Section III presents the testing of the platform and the experimental results basing on a dataset from 5 healthy subjects. Section IV concludes the paper.

2. The Architecture

The overall architecture can be divided into three sub-systems: (i) the acquisition unit, (ii) the processing unit and (iii) the navigation unit. The acquisition unit collects EEG data from the user and wirelessly (Bluetooth) sends them to the processing unit. The processing unit is the core of the systems, solving the main functions of the architecture i.e. (i) stimuli generation and delivery, (ii) data collection and synchronization, (iii) Machine Learning, (iv) real-time hyper-dimensional classification, (v) user intention

interpretation. Once the processing unit interprets the user's intent, it wirelessly (TCP/IP) sends the relative command to the navigation unit. The navigation unit is responsible for the command actuation and it controls the navigation through its sensors i.e. ultrasonic proximity sensors (for obstacle avoidance) and USB camera (for video processing/streaming). Figure 1 shows a high-level schematic of the developed BCI architecture.

2.1 The Acquisition Unit

The acquisition unit is a wireless (Bluetooth) 32-channels EEG headset. Conditioning integrated circuits are embedded in the electrodes performing "in loco" amplification, filtering and digitalization. Despite the employed acquisition unit is the one used in [16 - 21], the locations of the electrodes have been chosen according to previous P300 studies [24] and, in a later stage, reduced in number basing on the relevance in experimental conditions. EEG recordings are performed using six electrodes i.e. C_Z, CP_1, CP_2, P_3, P_z, P_4 (international 10-20 standard, see fig. 2.a). The recording scheme is monopolar. The reference electrode is AF_z while the right ear lobe (A_2) is used as ground. The filtering processing includes two stages: 2-30Hz bandpass (Butterworth, 8th order) and 48-52Hz notch (Butterworth, 4th order) filters. Both the filters are embedded into the acquisition front-end. The sampling rate is 500Hz with 24-bit resolution while the input range is ±187.5mV. Using a multiplexer, EEG data are directed to the 2.4 GHz Bluetooth XVV-MEGA22M00 module for the transmission. Figure 2.b present a schematic of the acquisition unit.

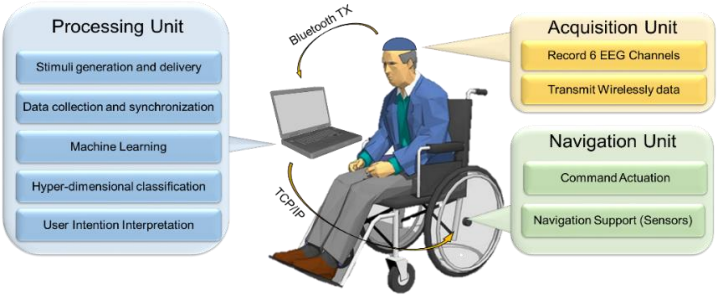

Fig. 1. Schematic overview of the developed BCI architecture.

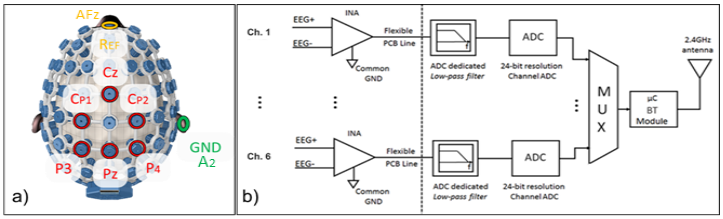

Fig. 2. a) Location of the electrodes recorded in this work; b) Schematic of the acquisition unit.

2.2 The Processing Unit

In our implementation, the processing unit is a PC (Intel i5, RAM 8 GB, 64 bit). The processing unit performs several functions in parallel and, for this reason, is the key part of the whole system.

Stimuli generation and delivery. The stimulation protocol is designed according to the oddball paradigm using visual stimuli. There are four delivered visual stimuli, individually and randomly flashing on a display (25% occurrence probability) with an inter-stimuli time of 1s. The stimulus persists on the screen for 200ms. Each stimulus is linked to a particular command to be sent to the navigation system i.e. start/go ahead, turn right, turn left, stop/go backwards. Neurophysiological studies [24] revealed that P300 latency and amplitude are related to the stimulus physiognomy (such as duration, contrast, color, etc.). For this reason, each command is linked to a different stimulus in terms of shape and color. Differently from a classic oddball paradigm, there is no pre-defined target stimulus. The user selects which stimulus is the target one, basing on his intention. Thus, only that particular stimulus, which is linked to the desired command, will evocate the P300. Figure 3 proposes a real example from our dataset (on C_Z electrode), showing the differences in the brain activity depending on the type of the stimulus. Only when a target stimulus is delivered, a clear positive peak rises approximately 300ms after the stimulus onset.

Data collection and Synchronization. The processing unit receives six real-time EEG signals from the acquisition unit by Bluetooth protocol. Subsequently, each channel undergoes a further filtering stage, aiming to reduce both noise and artifacts (eyes and head movements). The channels are pre-processed in parallel. The implemented numerical filter is a 6^{th} order low-pass Butterworth filter with f_{3dB} = 15Hz. The next pre-processing stage is the channels synchronization with the delivered stimuli. For this aim, filtered EEG signals are firstly decomposed in 1s segment (called – in this work – trial). The EEG trial starts as soon as the rising edge of the stimulation arrives. A 6^{th} order fitting polynomial of the evaluated trial is subtracted to the signal in order to center and scale the trial, without losing the P300 information. Finally, all the trials are organized into a 3D matrix DATA $\in R^{SxNxM}$ where S is the number of samples into a single trial (500 in our implementation), N is the number of monitored channels (6 in our work) and M is the number of delivered stimuli (target and not-target).

Machine Learning. The P300 latency is heavily affected by inter-subject and trial-to-trial variability and it ranges from 290ms to 447.5ms [3, 4, 11-14, 24]. Additionally, its amplitude is affected by high variability: it can reach even 37.7μV depending on the subject [3, 4, 11-14, 24].

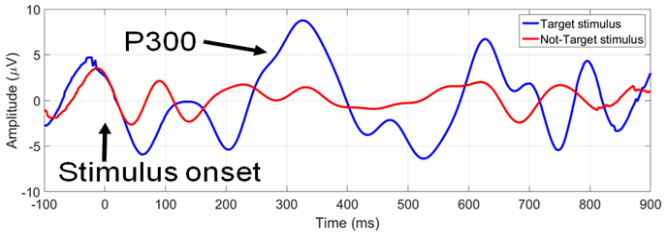

Fig. 3. The P300 can be detected only when a target stimulus is detected (Cz).

Due to this inter-subject variability, the system needs to be tuned on the particular user. The subject-optimization is achieved by a stage of Machine Learning (ML) to be performed on the first use of the system. In this case, the neurophysiological protocol delivered to the user is slightly different form the one above-described. In fact, the user performs a supervised oddball test targeting N known stimulus ($N \geq 22$ in our work, as demonstrated in section 3.2). For the ML stage, the processing is performed offline.

P300 Extraction for ML. The ML stage implemented in this BCI is based on a novel algorithm, named tuned-Residue Iteration Decomposition (t-RIDE). The improvements achieved by t-RIDE with respect to the state of the art for P300 extraction has been presented in [12]. In [12], it was demonstrated on a dataset of 12 subjects that (i) t-RIDE is 1.6 times faster than ICA (i.e., t-RIDE: 1.95s against ICA: 3.1s); (ii) t-RIDE reaches 80% of accuracy after only 13 targets; (iii) t-RIDE can be performed even on a single channel (differently from ICA). t-RIDE is a custom tuned version of RIDE [12] for P300 extraction which include three additional steps to RIDE: pre-processing, window optimization and spatial characterization. t-RIDE iteratively estimates the computation window which optimize the P300 extraction. Only one signal derived from the average of P_Z and C_Z is considered – at first - for window optimization. A first default window is defined as 250 - 400ms after the stimulus. The procedure for window optimization is based on an iterative approach. After n_{IT} iterations, the algorithm selects the optimized window i.e., the one with the highest P300 amplitude. As soon as the optimized window is defined, the DATA matrix is processed by t-RIDE. Time-domain results from each channel are subsequently interpolated in order to extract the spatial characterization (P300 topography). In this stage, the system stores the vectors $L = (l_1, \ldots, l_N) \in R^N$ and $A = (a_1, \ldots, a_N) \in R^N$ containing respectively the expected P300 latencies and amplitude for each channel ($N = 6$).

Feature Extraction (FE) for ML. The P300 pulse extracted by t-RIDE undergoes a phase of FE to be used as 'golden reference'. Basing on specialized medical guidelines and literature investigation, five features have been selected. For the FE on the j^{th} channel, the trial x(i) is windowed by a rectangular 200ms window (number of samples $n_s = 100$) centered on the expected latency l_j. The extracted features are:

1. The **Simmetry** quantifies the symmetry degree of the signal with respect to the expected latency:
$$f_1 = 1 - \left| \frac{2}{ns-1} \sum_{i=1}^{ns} [x(i) - x(ns-i)] \right| \quad (1)$$
2. The **Convexity** identifies the convexity degree of the considered data points with respect to the expected latency:
$$f_2 = 1 \leftrightarrow \sum_{i=1}^{\left(\frac{ns}{2}\right)-1} \frac{\partial x(i)}{\partial i} \geq \sum_{i=\left(\frac{ns}{2}\right)+1}^{ns} \frac{\partial x(i)}{\partial i} \; ; otherwise \quad f_2 = 0 \quad (2)$$
3. The **Triangle area (TA)** delivers the area of the triangle inscribed into the potentially P300 component deflection:
$$f_2 = 0.5 \cdot \begin{vmatrix} x1 & y1 & 1 \\ x2 & y2 & 1 \\ x3 & y3 & 1 \end{vmatrix} \quad (3)$$
where (x_1,y_1) is the minimum value in the 100ms before the P300 learned latency as well as (x_2, y_2) is the minimum value of the 100ms on its right side. (x_3, y_3) are the coordinates of maximum value of the extracted data points.
4. The **Peak to Max distance (PMD)** quantifies how close is the maximum point of the single trial with respect to the expected one:

$$f_4 = \left\{ \frac{(ns+1)}{2} - \left| \frac{(ns+1)}{2} - index(\max(x)) \right| \right\} \frac{2}{(ns+1)} \quad (4)$$

5. The **Direction changes index (DCI)** quantifies the number of considered waveform direction changes. It can be obtained by counting the slope sign changes, referring to signal derivative.

Thresholds/Weights Definition for ML. The features distributions are analyzed by a statistical method that extracts, for each feature and channel, the 25th and 75th percentiles and median value. A demonstrative picture for a generic feature is shown in Figure 4.a. Thresholds definition is based on the percentiles. The weights definition is based on the median values by evaluating the subtraction between the median value of the j-th feature vector referred to the target responses and the not-target ones (distance d in Figure 4.a). The learning step assigns their values in descending order starting from 0.3 for the best feature to 0.1 for the worst one. The remaining 3 features assume decreasing weights with 0.05 steps between 0.3 and 0.1. These values allow obtaining a sum that provides a maximum of 1.

Machine Learning Finalization. At the end of the ML and FE phase, the processing unit has learned the following subject-depending parameters:
(i) **UP** $\in R^{5x6}$ ($up_{i,j}$ = upper threshold for i-th feature referred to the j-channel);
(ii) **DN** $\in R^{5x6}$ ($dn_{i,j}$ = lower threshold for i-th feature referred to the j-channel);
(iii) **W** $\in R^{5x6}$ ($w_{i,j}$ = i-th weight referred to the j-channel)
(iv) **S** $\in R^{6}$: (s_j = responsivity - detection rate of the j-th channels);
(v) **L** $\in R^{6}$ (l_j = expected P300 latencies for the j-th channel);
(vi) **A** $\in R^{6}$ (a_j = expected P300 amplitude for the j-th channel).

Hyper-dimensional Real-Time Classification. For each subject, the "golden" learned P300 can be represented by a single point in a n-dimensional space where the features are the bases (n = number of features). Figure 4.b proposes a visual interpretation of the situation, supposing n=3. The real-time classifier performs a FE on incoming streaming EEG data and compares the results with the "golden" reference: the decision about the absence/presence of P300 is based on the n-dimensional distance between reference and incoming trial exploiting thresholds. In order to reduce the computational times, the classification is performed on a down-sampled (from 500sps to 100sps) and windowed (M samples centered on the expected latency, M = 20 ~200ms) version of EEG trials. The classifier implements 5 rules to decide presence/absence of the P300 component.

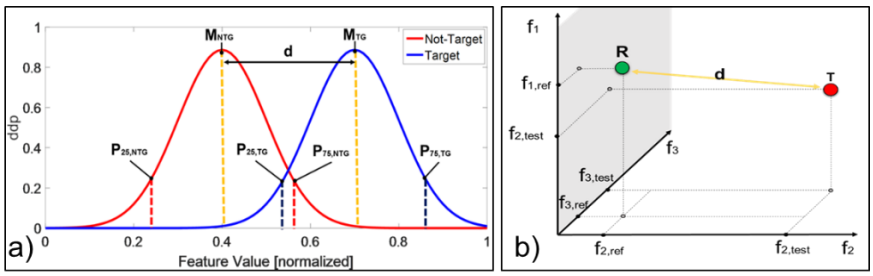

Fig. 4. a) Demonstrative picture of the statistical analysis performed during the ML. b) Visual interpretation of the classification approach (only 3 features for clarity).

When the classification is over, the processing unit sends to the navigation one a 2 bits code informing about the actuation through TCP/IP wireless communication.
1st rule: Data validation. Data are validated only if the they are similar in amplitude to the learned values in **A**:

Continue classification $\leftrightarrow \max(EEG_i) < ai + \varepsilon$ *otherwise* 'report error' and 'stop'
2nd rule: Single Feature on single channel. As soon as a new stimulus occurs, the processing unit performs the FE on the single-trial for each channel basing on **L**. This leads to the computation of $\mathbf{f} \in R^{5x6}$ where its generic element $f_{i,j}$ expresses the value of the i-th feature on the j-th channel. This procedure leads to the creation of the matrix $\mathbf{F} \in R^{5x6}$ adopting the following decisional rule:

$$F_{i,j} = \begin{cases} 0 & \leftrightarrow & f_{i,j} < dn_{i,j} \\ 0.5 & \leftrightarrow & dn_{i,j} \leq f_{i,j} \leq up_{i,j} \\ 1 & \leftrightarrow & f_{i,j} > up_{i,j} \end{cases} \quad (5)$$

3rd rule: *All features on single channels*. A weighted sum of **F** defines the presence of the P300 on the j-th channel, through the calculation of the vector $\mathbf{R} \in R^6$, where the generic element is:

$$r_j = w_{1,j} \cdot F_{1,j} + \ldots. + w_{5,j} \cdot F_{5,j} \text{ for } j = 1, 2, \ldots, 6 \quad (6)$$

4th rule: P300 presence/absence on single channel. Afterwards, the classifier adopts the a single threshold decision comparison to evaluate the presence/absence of P300 on the j-th channel:

$$y_j = \begin{cases} 0 & \leftrightarrow & r_j \leq y_t \\ 1 & \leftrightarrow & r_j > y_t \end{cases} \quad (7)$$

Where y_j is the generic element of $\mathbf{Y} \in R^6$ and y_t is a decision threshold set to 0.5. The rule yt =0.5 means that on the j-th channel, at least 3 features have been detected.
5th rule: P300 presence/absence on all the channels. The classifier validate the P300 presence only if the P300 is simultaneous detected on 5 out of 6 channels detect w.r.t. channels, which deliver a high detection rate (vector **S**).

2.3 The Navigation Unit

The navigation unit is responsible for (i) actuating the commands sent by the processing unit and (ii) supporting the navigation. The core of the navigation unit is Raspberry Pi 2 (Model B+) equipped by a Wi-Fi antenna (for the communication with the processing unit), an USB camera and a SD. Using a DC-DC converter (XL-1509), a nominal supply voltage of 7.4 V voltage is stabilized to 5V, delivering the power supply for the board. For actuating the commands sent by the processing unit, GPIO pins on Raspberry control the DC motor drivers. Particularly, two 12V DC motors are used in this work to demonstrate running of wheelchair in forward, reverse, left and right direction. L293D motor driver is used to interface with Raspberry Pi, which is TTL compatible. Two H bridges of L293D can be connected in parallel to increase its current capacity to 2A. Then, GPIO pins can be enable, disable or modulate (by PWM) the pins of the L293D. Finally, a relay is used to quickly change the motor direction. The PWM modulates with adequate set of cross-velocity the motor providing rotation. The rotation is possible along predefined destinations, in term of (distance, angle) couple that are relative to the wheelchair's location, which corresponded to locations in the environment that the participants might select to reach. For instance, a rotation on the left side is traduced in a couple (distance, angle) of (2m, -60°), while a right rotation reach the position (2m,

60°) starting from the initial position of the wheelchair. The PWM preset allows a maximum translational and rotational velocities of ω_{max} = 0.3 m/s and an average velocity of 0.16 m/s. On the other hand, two servomotors control the orientation of the USB camera, which streams a real-time video to the processing unit. The navigation unit supports the navigation by two different approaches: (i) obstacle avoidance and (ii) real-time modification of the neurophysiological protocol delivered to the user (w.r.t the protocol presented in section 2.2.1). The obstacle detection and avoidance is based on three ultrasonic proximity sensors (HC-SR04) which point in three different directions (straight and sideways): when an obstacle is detected ahead with a distance lower than 1m, the wheelchair stops. Differently, when the wheelchair detects a side obstacle that is not in its trajectory, Raspberry alerts the processing unit, which adapts the neurophysiological protocol preventing the choice of that specific direction. In this case, the processing unit does not deliver the visual stimuli linked to the command until further notice from the navigation unit. This procedure leads, de facto, to a modification of the oddball: the protocol is adaptive and is aware of the surroundings, proposing to the user only selections that are consistent with the environment. This approach, performing environment-related stimuli delivery, is a key-point of our platform and overcomes the static protocols presented in related works [2-10].

3 Experimental Results

The entire architecture has been tested on a dataset from 5 different subjects (age: 26 ± 3). The subjects performed at first the learning protocol and, subsequently, the real-time wheelchair control.

Machine Learning. In the testing stage, the neurophysiological paradigm for ML consist in a supervised oddball test (the target is known) presenting 30 target stimuli (i.e. 120s). The supervised oddball test is reiterated for each addressable direction and data are processed offline. The P300 amplitude range was 3 - 8μV with a mean value of 4.7μV ± 0.61μV; the P300 latency was included in the range 300 – 403ms, with a mean value of 349.25ms ± 35.52ms. Figure 5.a summarizes the overall accuracy considering the channel-to-channel responsivity (array named S). The boxplots in Figure 5.a have been obtained by statistically treating the responsivity of each channel, on 5 subjects. Considering the median values, the highest responsivity are reached by P_Z, C_Z, P_3, which obtain a value of 87.3%, 86.2%, 84.1%, respectively.

Real-time classification. The online validation approach included two different tests: (i) single direction repetitive selections and (ii) pattern recognition. In the first approach, the user is asked to select repeatedly a single target. The reached classification accuracies computed in these conditions are: sub_1: 73.68 ± 5.3 %; sub_2: 83.71 ± 4.6 %; sub_3: 80 ± 3.1 %; sub_4: 81.30 ± 4.8%; sub_5: 83.84 ± 5.8% (best: 89%, worst: 68.38%).

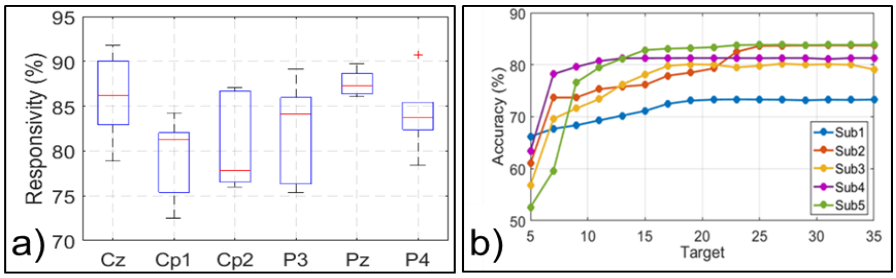

Fig. 5. a) Boxplot representation of the Responsivity vs. Electrode position; b) Accuracy (all the subjects) vs. n°. of target stimuli for training ;

Differently, the pattern recognition test consist in the selection of a known stream of directions (10 commands covering all the addressable directions). The performed accuracies computed in this test are: sub1: 67.9 ± 6.7 %; sub2: 72.5 ± 7.1 %; sub3: 67.5 ± 4.4 %; sub4: 69.2 ± 8.5 %; sub5: 70.6 ± 3.7% (best: 80% worst: 50%). Figure 5.b outlines the accuracy of the system as a function of the number of targets used to train the BCI. The graph shows separately the subjects accuracy. It is worth noting that, 4 subjects on 5 reaches the accuracy steady state by using only 15 target stimuli. It corresponds to a ML stage of about 60s for each direction. This lower limit is directly connected to the capability of the ML algorithm (t-RIDE) to reach the complete the P300 spatio-temporal characterization in the same number of targets (15 Targets → 90% of accuracy in P300 characterization) [12]. In the worst case, the system needs at least 22 targets (i.e. 88s) to recognize the intentions with an accuracy of 83.7% (Sub.2). The best case (Sub.4) requests only 10 targets and thus a ML duration of 40s/direction, obtaining an accuracy of 81.3%. From this analysis we can state that t-RIDE allows to drastically reduce the duration of the training, since it needs only 22 target stimuli for a worst-case complete characterization of P300 (88s). The shortening of the training phase allows reducing the effect of the "habituation" that typically spoils the P300. t-RIDE computational time was only 1.95s and it does not requires a minimum number of channels.

Timing. Since the application is in real-time, special attention should be devoted to timing in order to guarantee the correct functioning. The fixed communication latency from EEG headset and gateway is 14ms. The classifier needs to buffer 1s data after the stimulus in order to perform the computation. The worst-case computational time for each feature extraction on single channel and single trial was 0.653±0.32ms. The worst-case total time for the FE stage on 6 channels was 19.58±9.7ms. The successive definition of the matrix **F** was performed in 0.026±0.011ms on all the channels. The computational time (for 6 channels) for the spatial validation was 0.041±0.008ms. Given this computational details, the worst-case total time needed by the classifier to complete the classification for all the channels was 19.65 ± 10.1ms. The FE stage is the most time consuming part of the process. The communication time between processing and navigation unit takes about 3.35ns (only 2 bits to be sent by Wi-Fi). As soon as Raspberry Pi receives the command, the actuation is performed in 3ms (worst-case). The overall architecture complete a single actuation (from EEG raw data acquisition triggered by stimulus delivery to PCS actuation) in 1.03s (worst-case). Timing is not related to the subject but figure 6 highlights the variability of this parameter.

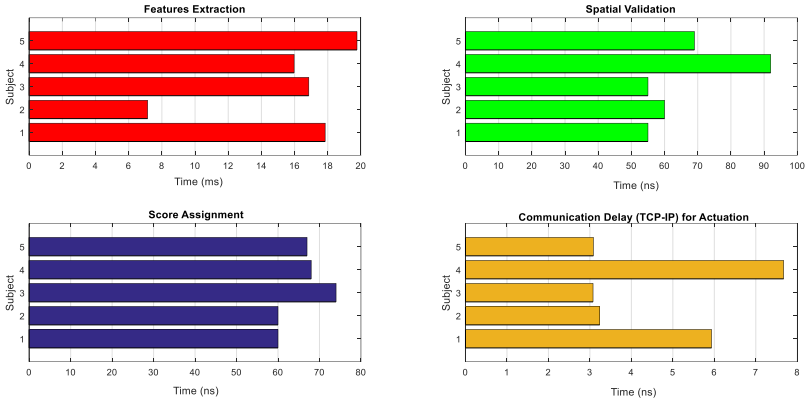

Fig. 6. Timing details for different tasks performed by the classifier.

4 Conclusion

The aim of the present work was the study, the design, implementation and test of a brain-computer interface based on P300. The implemented neural interface allows remote control of a wheelchair. The ML stage is based on the custom algorithm t-RIDE, which trains the following hyper-dimensional real-time classifier performing in real time the FE on raw data for the detection of presence/absence of P300. The system has been validated on a dataset of 5 subjects driving the wheelchair by their mind. The average classification accuracy on a single direction was 80.51 ± 4.1 %. The average classification accuracy in the detection of a 10-direction pattern was 69.6 ± 1.9 %. The classifier completes its process on all the channels in 19.65± 10.1ms (worst-case). According to the achieved results, the oddball protocol used for training can be reduced to 88s/direction (worst case). The computational time for ML is 1.95s. Future perspectives include the use of biocompatible and flexible electronics in order to increase the wearability degree of the system [25, 26], the optimization of the wireless network [27-30] and the design and fabrication of an Application Specific Integrated Circuit (ASIC) [31-35].

References

1. Graimann, Bernhard, Brendan Allison, and Gert Pfurtscheller. "Brain–computer interfaces: A gentle introduction." Brain-Computer Interfaces. Springer Berlin Heidelberg, 2009.
2. Grychtol, B., Lakany, H., Valsan, G., & Conway, B. A. (2010). Human behavior integration improves classification rates in real-time BCI. Neural Systems and Rehabilitation Engineering, 8(4), 362-368. doi: 10.1109/TNSRE.2010.2053218
3. De Venuto, D., Vincentelli, A.S. “Dr. Frankenstein's dream made possible: Implanted electronic devices”. Proceedings -Design, Automation and Test in Europe, DATE, art. no. 6513757, pp. 1531-1536. 2013.

4. De Venuto, D., Annese, V.F., Mezzina, G. "An Embedded System Remotely Driving Mechanical Devices by P300 Brain Activity". Proceedings of the 2017 Design, Automation and Test in Europe Conference and Exhibition, DATE 2017. ISBN: 978-3-9815370-8-6.
5. Ortner, R. et al. "An SSVEP BCI to control a hand orthosis for persons with tetraplegia." IEEE Transactions on Neural Systems and Rehabilitation Engineering 19.1 (2011): 1-5.
6. Barnes, N. (2012). Visual processing for the bionic eye: Research and development of visual processing for low vision devices and the bionic eye.
7. Farwell, L.A., & Donchin, E. (1988). Talking off the top of your head: Toward a mental prosthesis utilizing event-related brain potentials. Electroenceph Clin Neurophysiol, 70(6), 510-523. dio:1988;70:510–523
8. Hochberg, L. R., et al. Neuronal ensemble control of prosthetic devices by a human with tetraplegia. Nature Journal 442, 164–171.
9. Nijholt, Anton. "BCI for games: A 'state of the art'survey." International Conference on Entertainment Computing. Springer Berlin Heidelberg, 2008.
10. Fernando, L., Alonso, N., & Gomez-Gil, J. (2012). Brain computer interfaces, a review. Sensors, 12(2), pp.1211-1264.
11. De Tommaso, M., Vecchio, E., Ricci, K., Montemurno, A., De Venuto, D., Annese, V.F. "Combined EEG/EMG evaluation during a novel dual task paradigm for gait analysis". Proceedings - 2015 6th IEEE International Workshop on Advances in Sensors and Interfaces, IWASI 2015, art. no. 7184949, pp. 181-186. DOI: 10.1109/IWASI.2015.7184949. 2015.
12. De Venuto, D., Annese, V.F., Mezzina, G. "Remote Neuro-Cognitive Impairment Sensing based on P300 Spatio-Temporal Monitoring". IEEE Sensors Journal, PP (99), art. no. 7562544. DOI: 10.1109/JSEN.2016.2606553. 2016.
13. Annese, V.F., Mezzina, G., De Venuto, D. "Towards mobile health care: Neurocognitive impairment monitoring by BCI-based game". Proceedings of IEEE Sensors, art. no. 7808745. DOI: 10.1109/ICSENS.2016.7808745. 2017.
14. De Venuto, D., Annese, V.F., Mezzina, G., Ruta, M., Sciascio, E.D. "Brain-computer interface using P300: A gaming approach for neurocognitive impairment diagnosis". 2016 IEEE International High Level Design Validation and Test Workshop, HLDVT 2016, art. no. 7748261, pp. 93-99. DOI: 10.1109/HLDVT.2016.7748261. 2016.
15. Fernández-Rodríguez, Á., Francisco Velasco-Álvarez, and R. Ron-Angevin. "Review of real brain-controlled wheelchairs." Journal of Neural Engineering 13.6 (2016): 061001.
16. Annese, V.F., De Venuto, D. "Gait analysis for fall prediction using EMG triggered movement related potentials". Proceedings - 2015 10th IEEE International Conference on Design and Technology of Integrated Systems in Nanoscale Era, DTIS 2015, art. no. 7127386. DOI: 10.1109/DTIS.2015.7127386. 2015.
17. De Venuto, D., Annese, V.F., Ruta, M., Di Sciascio, E., Sangiovanni Vincentelli, A.L. "Designing a Cyber-Physical System for Fall Prevention by Cortico-Muscular Coupling Detection". IEEE Design and Test, 33 (3), art. no. 7273831, pp. 66-76. DOI: 10.1109/MDAT.2015.2480707. 2016.
18. Annese, V.F., De Venuto, D. "Fall-risk assessment by combined movement related potentials and co-contraction index monitoring". IEEE Biomedical Circuits and Systems Conference: Engineering for Healthy Minds and Able Bodies, BioCAS 2015 - Proceedings, art. no. 7348366. DOI: 10.1109/BioCAS.2015.7348366. 2015.
19. Annese, V.F., De Venuto, D. "FPGA based architecture for fall-risk assessment during gait monitoring by synchronous EEG/EMG". Proceedings - 2015 6th IEEE International Workshop on Advances in Sensors and Interfaces, IWASI 2015, art. no. 7184953, pp. 116-121. DOI: 10.1109/IWASI.2015.7184953. 2015.
20. Annese, V.F., Crepaldi, M., Demarchi, D., De Venuto, D. "A digital processor architecture for combined EEG/EMG falling risk prediction". Proceedings of the 2016 Design, Automation and Test in Europe Conference and Exhibition, DATE 2016, art. no. 7459401, pp. 714-719. 2016.
21. Annese, V.F., De Venuto, D. "The truth machine of involuntary movement: FPGA based cortico-muscular analysis for fall prevention".2015 IEEE International Symposium on

Signal Processing and Information Technology, ISSPIT 2015, art. no. 7394398, pp. 553-558. DOI: 10.1109/ISSPIT.2015.7394398. 2015.
22. De Venuto, D., Annese, V.F., Sangiovanni-Vincentelli, A.L. “The ultimate IoT application: A cyber-physical system for ambient assisted living”. Proceedings - IEEE International Symposium on Circuits and Systems, 2016-July, art. no. 7538979, pp. 2042-2045. DOI: 10.1109/ISCAS.2016.7538979. 2016.
23. De Venuto, D., Annese, V.F., Defazio, G., Gallo, V.L., Mezzina, G. "Gait Analysis and Quantitative Drug Effect Evaluation in Parkinson Disease by Jointly EEG-EMG Monitoring". Proceedings - 2017 12th IEEE International Conference on Design and Technology of Integrated Systems in Nanoscale Era, DTIS 2017.
24. S.H. Patel and P.N. Azzam, “Characterization of N200 and P300:Selected Studies of the Event-Related Potential”, International Journal of Medical Sciences, pp. 147–154, October 2005.
25. Annese, V.F., De Venuto, D., Martin, C., Cumming, D.R.S. “Biodegradable pressure sensor for health-care”. 2014 21st IEEE International Conference on Electronics, Circuits and Systems, ICECS 2014, art. no. 7050056, pp. 598-601. DOI: 10.1109/ICECS.2014.7050056. 2014.
26. Annese, V.F., Martin, C., Cumming, D.R.S., De Venuto, D. “Wireless capsule technology: Remotely powered improved high-sensitive barometric endoradiosonde”. Proceedings - IEEE International Symposium on Circuits and Systems, 2016-July, art. no. 7527504, pp. 1370-1373. DOI: 10.1109/ISCAS.2016.7527504. 2016.
27. Annese, V.F., De Venuto, D. “On-line shelf-life prediction in perishable goods chain through the integration of WSN technology with a 1st order kinetic model”. 2015 IEEE 15th International Conference on Environment and Electrical Engineering, EEEIC 2015 - Conference Proceedings, art. no. 7165232, pp. 605-610. DOI: 10.1109/EEEIC.2015.7165232. 2015.
28. Annese, V.F., Biccario, G.E., Cipriani, S., De Venuto, D. “Organoleptic properties remote sensing and life-time prediction along the perishables goods supply-chain”. Proceedings of the International Conference on Sensing Technology, ICST, 2014-January, pp. 130-135. 2014.
29. De Venuto, D., Annese, V. F., de Tommaso, M., Vecchio, E., and Vincentelli, A. S. "Combining EEG and EMG signals in a wireless system for preventing fall in neurodegenerative diseases." Ambient Assisted Living. Springer International Publishing. pp 317-327. 2015.
30. Biccario, G.E., Annese, V.F., Cipriani, S., De Venuto, D. “WSN-based near real-time environmental monitoring for shelf life prediction through data processing to improve food safety and certification” ICINCO 2014 - Proceedings of the 11th International Conference on Informatics in Control, Automation and Robotics, 1, pp. 777-782. 2014.
31. De Venuto, D., Carrara, S., Ricco, B. “Design of an integrated low-noise read-out system for DNA capacitive sensors”. Microelectronics Journal, 40 (9), pp. 1358-1365. DOI: 10.1016/j.mejo.2008.07.071. 2009.
32. De Venuto, D., Castro, D.T., Ponomarev, Y., Stikvoort, E. “Low power 12-bit sar adc for autonomous wireless sensors network interface”. 3rd International Workshop on Advances in Sensors and Interfaces, IWASI 2009, art. no. 5184780, pp. 115-120. DOI: 10.1109/IWASI.2009.5184780. 2009.
33. De Venuto, D., Ohletz, M.J., Ricco, B. “Automatic repositioning technique for digital cell based window comparators and implementation within mixed-signal DfT schemes”. Proceedings – International Symposium on Quality Electronic Design, ISQED, 2003-January, art. no. 1194771, pp. 431-437. DOI: 10.1109/ISQED.2003.1194771. 2003.
34. De Venuto, D., Ohletz, M.J., Ricco, B. “Digital window comparator DfT scheme for mixed-signal ICs”. Journal of Electronic Testing: Theory and Applications (JETTA), 18 (2), pp. 121-128. DOI: 10.1023/A:1014937424827. 2002.
35. De Venuto, D., Ohletz, M.J., Ricco, B. “Testing of analogue circuits via (standard) digital gates”. Proceedings - International Symposium on Quality Electronic Design, ISQED, 2002-January, art. no. 996709, pp. 112-119. DOI: 10.1109/ISQED.2002.996709. 2002.